CHEMISTRY OF MATERIALS

ARTICLE

pubs.acs.org/cm

$YCa_3(VO)_3(BO_3)_4$: A Kagomé Compound Based on Vanadium(III) with a Highly Frustrated Ground State

Wojciech Miiller,[†,‡] Mogens Christensen,[‡,∥] Arfhan Khan,[†] Neeraj Sharma,[†,⊥] René B. Macquart,[†] Maxim Avdeev,[‡] Garry J. McIntyre,[§,⊥] Ross O. Piltz,[‡] and Chris D. Ling*[,†]

[†]School of Chemistry, The University of Sydney, Sydney 2006, Australia

[‡]Bragg Institute, ANSTO, Locked Bag 2001, Kirrawee DC 2232, Australia

[§]Institute Laue Langevin, 6, rue Jules Horowitz, BP 156, 38042 Grenoble CEDEX 9, France

Supporting Information

ABSTRACT: A new $S = 1$ kagomé compound based on vanadium(III) is reported. The structure was refined simultaneously against single-crystal neutron and X-ray diffraction data, as a gaudefroyite-type with a new supercell ($\mathbf{a}' = 2\mathbf{a} + \mathbf{b}$, $\mathbf{b}' = -\mathbf{a} - 2\mathbf{b}$, $\mathbf{c}' = \mathbf{c}$) driven by the ordering of columns of isolated triangular BO_3^{3-} ions. Low-temperature neutron powder diffraction and magnetic (dc and ac susceptibility) data rule out the presence of long-range magnetic order above at least 1.5 K, but specific heat data suggest that the ground state involves short-range magnetic order, which is frustrated by the coexistence/competition of FM and AFM correlations, together with the characteristic geometric frustration of the kagomé lattice. Magnetic susceptibility data rule out a spin-glass state, pointing to an exotic ground state comparable to the spin-ice or spin-liquid states. This makes $YCa_3(VO)_3(BO_3)_4$ one of the most highly frustrated experimental realizations of the kagomé lattice yet discovered.

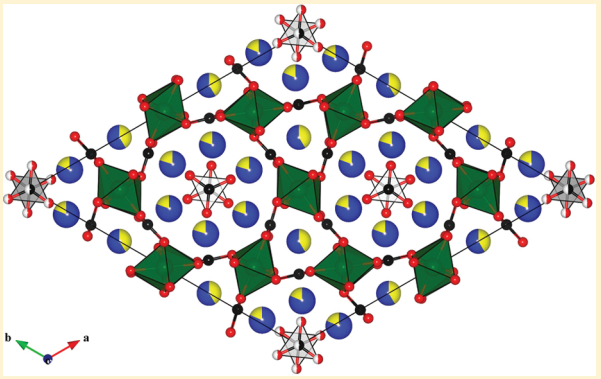

KEYWORDS: kagomé lattice, gaudefroyite structure, vanadium(III), single crystal growth, neutron Laue diffraction, magnetic frustration, borate

INTRODUCTION

If magnetic cations are arranged on a triangular lattice in a layered crystal structure and interact antiferromagnetically (AFM), it is impossible for the spins of the three cations on the vertices to be simultaneously antiparallel to one another. This results in a macroscopic number of degenerate ground states, a situation referred to as geometrically frustrated magnetism. The frustration may be resolved by some perturbation that breaks the degeneracy, either internal (e.g., phase transition, second-nearest-neighbor interactions) or external (e.g., magnetic field, pressure); but if not, the spins will in principle continue to fluctuate down to 0 K. This quantum spin-liquid[1,2] state is of fundamental importance to the study of magnetism and particularly for high-temperature superconductivity, where conventional magnetic order may be suppressed by similar quantum fluctuations.[3] Alternatively, as thermal fluctuations decrease upon cooling, regions of short-range-order may be frozen into the lattice, resulting in a spin-glass state. Spin glasses have a large number of possible low-energy configurations separated by very small energy differences, and their low-temperature relaxation is unusually slow and dependent upon external conditions and history. Spin glasses are archetypes of complex behavior and have been used as models in economics, evolutionary biology, and neural networks.

The kagomé lattice, which consists of corner-connected triangles that form a larger infinite hexagonal array, is one of the basic structural motifs that can lead to geometrically frustrated magnetism. Furthermore, the archetypal three-dimensional geometrically frustrated magnetic lattice —the pyrochlore-type— can be constructed from four interpenetrating kagomé lattices, where the triangles form the faces of corner-connected tetrahedra. The low-temperature physics of magnetic kagomé compounds are therefore of significant interest. A promising approach to finding new examples of "pure" kagomé compounds is to make use of triangular (or tetrahedral) linker units to connect magnetic cations. The jarosite-type compounds $AM_3(SO_4)_2(OH)_6$ (A = Na^+, K^+, Rb^+, Tl^+; M = Fe^{3+}, Cr^{3+}, V^{3+}), containing tetrahedral SO_4^{2-} linker units are the best examples,[4−6] although these suffer from significant nonstoichiometry on the transition

Received: November 27, 2010
Revised: January 9, 2011
Published: January 31, 2011

metal sites (≥2% M vacancies), which complicates the interpretation and reproducibility of magnetic properties. The triangular borate group BO_3^{3-} is another linker unit that has been used to prepare a kagomé compound, $YCa_3(MnO)_3(BO_3)_4$, which is fully stoichiometric.[7] This compound has a structure related to the mineral gaudefroyite, $Ca_4(MnO)_3(BO_3)_3CO_3$.[8] It contains magnetic Mn^{3+} ions in MnO_6 octahedra, which are linked by sharing vertices with BO_3 units to form a perfect two-dimensional kagomé lattice. The fourth BO_3^{3-} ion (CO_3^{2-} in gaudefroyite) *per* formula unit lies in the middle of the hexagon formed by the kagomé lattice, either slightly above or below its plane (in a disordered statistical distribution). Perpendicular to this plane, the MnO_6 octahedra share edges to form chains.

Low-temperature magnetic and neutron powder diffraction experiments show that the Mn^{3+} (d^4, $S = 2$) ions in $YCa_3(MnO)_3(BO_3)_4$ couple ferromagnetically (FM) along the infinite chain direction, and that these chains themselves order into the $q = 0$ (i.e., the nuclear and magnetic unit cells are identical) noncolinear AFM kagomé structure below 7.5 K. This was a somewhat surprising result. Although the ∼90° Mn−O−Mn superexchange interactions along the chain are expected to be FM according to the Goodenough-Kanamori rules, in practice, edge-shared MnO_6 octahedra usually give rise to AFM superexchange, e.g., in MnO,[9] $LiMnBO_3$,[10] and $CaMn_2O_4$.[11] After carefully considering the Mn−O−Mn bond lengths and angles, the role of O bonding to B, and the possibility of direct Mn−Mn orbital overlap, Li and Greaves[7] concluded that the chains in $YCa_3(MnO)_3(BO_3)_4$ could only be FM if d electrons were delocalized along those chains in a double-exchange mechanism. However, resistivity measurements on single crystals indicated that the chains are insulating.

A subsequent investigation of a sample of natural gaudefroyite, $Ca_3(MnO)_3(BO_3)_3CO_3$, found similar FM interactions along the edge-sharing MnO_6 octahedral chains.[8] However, in this case, the geometric frustration in the kagomé planes appears to be stronger; no long-range magnetic order was observed down to 1.8 K, with the compound behaving as a spin glass below 10 K.

The unusual magnetic behavior of $YCa_3(MnO)_3(BO_3)_4$ and $Ca_4(MnO)_3(BO_3)_3CO_3$ means that it would be of considerable interest to study further compounds with the same topology but a different transition metal. In this light, we report here the synthesis, structure, and magnetic properties of gaudefroyite-type $YCa_3(VO)_3(BO_3)_4$.

EXPERIMENTAL SECTION

Samples of $YCa_3(VO)_3(BO_3)_4$ were synthesized from commercially available polycrystalline Y_2O_3, $CaCO_3$, V_2O_5, and B_2O_3, all of 99.99% or higher purity. $CaCO_3$ was dried at 900 °C overnight prior to use. An approximately 3 g of mixture of the correct stoichiometry in terms of cation ratios—with the exception of B_2O_3, which was used in 10% excess—was ground together in an agate mortar and pestle, placed in an alumina crucible, and heated in air to 500 °C for 10 h. The sample was cooled, reground, heated in a tube furnace to 1000 °C under an atmosphere of flowing 3.5% H_2 (balance Ar) for 1 week, and then furnace cooled to room temperature. Upon removal from the furnace, the sample consisted of a large number of heavily intergrown black plate-like crystals approximately 1 mm across and 0.1 mm thick, embedded in a smooth and shiny black matrix that had coated the entire inside surface of the crucible and appeared to have acted as a flux. This entire mass was extremely hard, and crystals could only be extracted by breaking them (including the crucible) apart with a hammer.

From the intergrown appearance of the plates in the grown mass, we did not expect to find useful single crystals larger than ∼0.1 mm. However, preliminary neutron Laue patterns collected on the diffractometer VIVALDI[12] at the Institut Laue-Langevin, France, showed that large numbers of these intergrown plates were in fact part of the same domain, yielding single crystals up to 3 mm in diameter. Complete single-crystal neutron Laue diffraction data sets were subsequently collected on the instrument Koala at the OPAL research reactor, ANSTO, Australia. Like VIVALDI, Koala uses a "white" thermal-neutron beam (0.8 Å ≤ λ ≤ 5.2 Å) and a cylindrical image-plate detector. A roughly spherical ∼1 mm diameter crystal mounted on an aluminum pin was used for data collection on both instruments. Neutron Laue patterns were collected on Koala in 12 exposures of 2 h each, separated by 12° rotations of the φ-axis (perpendicular to the neutron beam), providing good data redundancy and completeness. Complete data sets were collected at room temperature, 150, and 3 K. Reflections were indexed using the program LAUEGEN,[13,14] integrated using ARGONNE_BOXES,[15] and normalized to the wavelength distribution of the neutron beam using LAUENORM.[16] Experimental details are recorded in Table 1. One of the 150 K diffraction patterns collected on Koala is shown in Figure 1.

Single-crystal X-ray diffraction data were collected from a smaller (∼0.1 mm diameter) crystal on a Bruker-Nonius FR591 Kappa Apex II diffractometer, using MoK_α (λ = 0.71073 Å) radiation from a rotating anode generator. Data were collected at 150 K and cooled with the Oxford 700+ cryostream. Data were collected over 24 h. A full sphere of data was collected for $\sin\theta/\lambda \leq 1.2$. Indexing was carried out using the Bruker-Nonius *Cell Now* program, and an absorption correction was performed using the Bruker-Nonius *TwinAbs* program. Experimental details are recorded in Table 1.

Li and Greaves[7] observed additional NPD intensity at low q for $YCa_3(MnO)_3(BO_3)_4$ below 7.5 K, due to the appearance of long-range-ordered magnetism. However, Laue diffraction is not ideally suited to the search for such increases because of its incomplete coverage and chromatic overlap low q. A more suitable technique is neutron powder diffraction (NPD). High-resolution NPD data were therefore collected on the instrument Echidna at the OPAL research reactor, ANSTO, Australia. In order to minimize absorption by the ^{10}B isotope in natural boron, a second sample was synthesized in the same manner as described above, but using isotopically pure $^{11}B_2O_3$. The sample was mechanically separated from the crucible and ground to a powder. Unfortunately, it was not possible to separate completely the single crystals from the matrix, and X-ray powder diffraction data collected on a laboratory instrument revealed that the resulting 1 g of powder sample contained small amounts of V_2O_3, CaB_2O_4, and YBO_3 as impurities. NPD data were collected from a 1 g sample placed in a 6 mm diameter vanadium can and data collected over 4 h per temperature at 300, 50, and 1.5 K. A relatively long wavelength of 2.4395 Å was used in order to focus on the low-q region of the diffraction patterns, where any additional low-temperature peaks due to long-range magnetic order would be observed.

DC magnetic susceptibility and magnetization data were collected on a Physical Property Measurement System (PPMS, Quantum Designs), using the vibrating sample technique in magnetic fields up to 9 T over the temperature range of 3−300 K. We used the ac magnetic susceptibility (ACMS) probe to measure ac susceptibility with a magnetic field amplitude of 2 Oe and a frequency f = 1−10 kHz at temperatures above 2 K. Both ac and dc magnetic data were collected on a few selected and nonoriented crystals. Specific heat measurements were carried on the same platform over the temperature range 1.8−150 K.

RESULTS

Visual inspection of the room-temperature neutron Laue patterns during the indexing procedure made it immediately

Table 1. Single-Crystal Neutron Laue and X-ray Diffraction Data Collection and Refinement Details for $YCa_3(VO)_3(BO_3)_4$ in the Hexagonal Space Group $P\bar{3}$ (#147)

data	X-ray (MoK_α)	neutron (Laue)	combined
temperature (K)	150	150	
a (Å)	18.1995(9)		
c (Å)	5.7954(3)		
V (Å^3)	1662.39(8)		
Z	1		
λ (Å)	0.71073	0.9−2.0	
crystal volume (mm^3)	0.001	0.5	
no. reflections	6474	9908	
no. observed reflections [$I > 3\sigma(I)$]	2561	2418	
R_{obs} from σ(I)	0.0223	0.0801	
no. refined parameters	149	149	150
no. of constraints	42	42	42
R_{obs}	0.0297	0.1346	0.1033
wR_{obs}	0.0347	0.1136	0.0577
goodness-of-fit	1.70	2.72	2.22

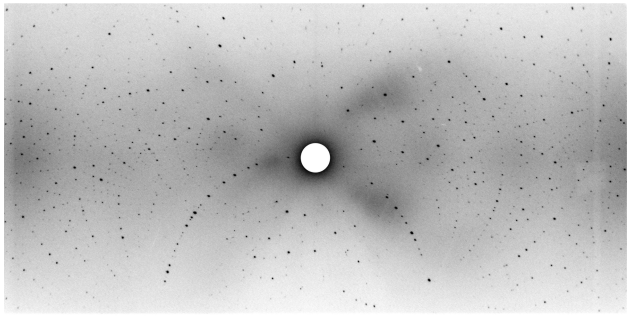

Figure 1. Typical single-crystal neutron Laue diffraction pattern of $YCa_3(VO)_3(BO_3)_4$, collected at 150 K on the Koala diffractometer at OPAL, ANSTO. The transmitted incident neutron beam exits the detector through the central hole, and the weak diffuse scattering in the central region is white-beam powder diffraction from the polycrystalline aluminum cryostat heat shields. All discrete spots could be indexed to $YCa_3(VO)_3(BO_3)_4$.

clear that the standard hexagonal ($P6_3/m$) $a \approx 10.6$, $c \approx 5.9$ Å unit cell of gaudefroyite[17,18] could not account for all observed Bragg reflections. It was necessary to enlarge the a axis by a factor of $3^{1/2}$ and rotate by 90° to remove all systematic extinction conditions before the patterns could be completely indexed. The resulting supercell has hexagonal $P\bar{3}$ space group symmetry and is related to the conventional cell of gaudefroyite (and for $YCa_3(MnO)_3(BO_3)_4$) by $\mathbf{a}' = 2\mathbf{a} + \mathbf{b}$, $\mathbf{b}' = -\mathbf{a} - 2\mathbf{b}$, $\mathbf{c}' = \mathbf{c}$. Both neutron and X-ray diffraction data were indexed and integrated in this supercell.

The fact that no such supercell was observed in previous X-ray diffraction studies of gaudefroyite-type structures and the extremely weak intensities of the supercell reflections in our own X-ray data (compared to our neutron data), suggests ordering of the relatively light boron atoms. Indeed, the BO_3 triangles stacked in columns in the smaller unit cell all show occupational disorder, with a 50% probability of lying either slightly above or below the kagomé plane. Our supercell contains three, rather than only one, such columns and permits two of them to be ordered, with the BO_3 triangles of the first column all lying above the plane and those of the second column all lying below. In a recurrence of the theme of geometric frustration in this compound, the third column at (0, 0, z) cannot be different to both of the others at the same time, and must therefore retain the occupational disorder of the subcell.

Structural refinements were carried out using the Jana2006[19] package. The supercell described above was used as the starting model, incorporating the model of Li and Greaves[7] for antisite disorder between the Ca and Y sites in $YCa_3(MnO)_3(BO_3)_4$. The model was refined simultaneously against neutron and X-ray diffraction data, both collected at 150 K. Simultaneous refinements such as these are rarely attempted because of difficulties with scaling and weighting between the data sets, which generally have very different characteristics in terms of spatial resolution, counting statistics, and numbers of observed reflections. Although these difficulties were also encountered in the present case, the combined refinement was necessary to obtain a reliable result, in a textbook case of X-ray and neutron complementarity. Because X-ray scattering is in direct proportion to the atomic number, boron (and, to a lesser extent, oxygen) atoms make virtually no contribution to the X-ray data, which are dominated by the much heavier metal cations. Neutron scattering length is not proportional to the atomic number, so boron and oxygen (scattering length = 5.30 and 5.80 fm, respectively) scatter on the same scale as calcium and yttrium (scattering length = 4.70 and 7.75 fm, respectively). However, vanadium is an extremely weak neutron scatterer (scattering length = −0.38 fm) and so makes virtually no contribution to the neutron data. Only a combined refinement could allow us to refine freely all the structural parameters in $YCa_3(VO)_3(BO_3)_4$. Refinement details are presented in Table 1, with the refined structure details presented in Table 2 and the refined structure shown in Figure 2 (drawn using the program VESTA[20]). Further structural and refinement details, including anisotropic atomic displacement parameters (ADPs), are contained in the deposited CIF file in the Supporting Information. Empirical bond-valence sums[21] (BVS) reported in Table 2 take into account the local structure in the disordered BO_3^{3-} column, i.e., the fact that entire triangles (either $B4O5_3$ or $B5O9_3$) must be present. The BVS for B4, for example, is therefore calculated on the basis that the O5 site is 100%

dx.doi.org/10.1021/cm1034003 |*Chem. Mater.* 2011, 23, 1315–1322

Table 2. Structural Details for $YCa_3(VO)_3(BO_3)_4$ at 150 K, Refined against Single-Crystal Neutron Laue and X-ray Diffraction Data[a]

atom	x (a)	y (b)	z (c)	100 $U_{iso/eq}$ (Å^3)	occupancy	BVS[21]
B1	0.1061(3)	0.6679(3)	0.2505(7)	0.080(16)†	1	2.91(2)
B2	0.4407(2)	0.3357(3)	0.2480(7)	0.080(16)†	1	2.91(2)
B3	0.7724(2)	0.0008(3)	0.2513(7)	0.080(16)†	1	2.91(2)
B4	0	0	0.907(2)	0.080(16)†	0.5	2.984(19)
B5	0	0	0.410(2)	0.080(16)†	0.5	2.889(19)
B6	0.333333	0.666667	0.9096(12)	0.080(16)†	1	2.908(16)
B7	0.333333	0.666667	0.4086(12)	0.080(16)†	1	2.914(15)
O1	0.95751(17)	0.74269(17)	0.4591(5)	0.36(6)	1	2.042(14)
O2	0.29150(17)	0.40592(16)	0.4570(5)	0.29(5)	1	2.062(14)
O3	0.62288(17)	0.07837(17)	0.4601(5)	0.46(6)	1	2.003(13)
O4	0.9286(3)	0.0086(3)	0.4039(10)	0.47(11)	0.5	1.991(13)
O5	0.26182(16)	0.67530(15)	0.4040(5)	0.21(5)	1	1.973(9)
O6	0.37505(16)	0.92692(17)	0.9574(5)	0.32(6)	1	2.096(14)
O7	0.71001(16)	0.58808(16)	0.9587(5)	0.26(5)	1	2.009(13)
O8	0.04284(18)	0.25859(18)	0.9588(5)	0.48(6)	1	2.010(13)
O9	0.0708(3)	0.9914(3)	0.9048(9)	0.22(10)	0.5	1.956(12)
O10	0.40495(16)	0.65813(16)	0.9045(5)	0.37(5)	1	1.968(9)
O11	0.09451(17)	0.81252(17)	0.7512(5)	0.36(5)	1	2.207(9)
O12	0.42691(18)	0.47916(19)	0.7515(5)	0.43(6)	1	2.184(9)
O13	0.76028(17)	0.14493(18)	0.7471(5)	0.44(6)	1	2.192(9)
O14	0.74672(17)	0.91458(17)	0.2489(5)	0.27(6)	1	2.026(15)
O15	0.08047(18)	0.58075(18)	0.2484(5)	0.32(6)	1	2.022(14)
O16	0.41339(16)	0.24781(17)	0.2530(5)	0.22(5)	1	1.997(14)
V1	0.66626(6)	0.83274(6)	−0.00090(16)	0.54(2)	1	3.363(13)
V2	0.66710(6)	0.83388(6)	0.49948(16)	0.54(2)	1	3.384(13)
V3	0	0.5	0	0.54(4)	1	3.364(12)
V4	0	0.5	0.5	0.55(4)	1	3.340(12)
Y1/Ca1	0.66671(5)	−0.00003(5)	0.74996(7)	0.46(2)	0.414(3)/ 0.586(3)	2.810(9)/ 2.442(8)
Y2/Ca2	0.19702(5)	0.67907(5)	0.74318(12)	0.52(3)	0.196(3)/ 0.804(3)	2.404(9)/ 2.089(8)
Y3/Ca3	0.53046(5)	0.34585(5)	0.75644(12)	0.57(3)	0.204(3)/ 0.796(3)	2.415(9)/ 2.098(8)
Y4/Ca4	0.86368(5)	0.01244(5)	0.75024(14)	0.52(3)	0.185(6)/ 0.815(6)	2.357(11)/ 2.048(9)

[a] Superscript symbols indicate constraints. Space group: hexagonal $P\bar{3}$ (#147); a = 18.1995(9), and c = 5.7954(3) Å.

occupied and the O9 site 0% occupied, even though they are statistically both 50% occupied.

As noted earlier, Li and Greaves[7] observed additional NPD intensity at low q for $YCa_3(MnO)_3(BO_3)_4$ below 7.5 K due to the long-range magnetic ordering. To search for similar ordering in $YCa_3(VO)_3(BO_3)_4$, we compared low-q NPD data at 50 to 1.5 K, as shown in Figure 3. As discussed in the Experimental Methods section, the sample used to collect these data contained a V_2O_3 impurity (in addition to CaB_2O_4 and YBO_3), which gives rise to the magnetic peak marked with an asterisk (∗). Nevertheless, the remaining peaks in this region of the pattern can be indexed to $YCa_3(VO)_3(BO_3)_4$, and no additional intensity is observed in these peaks at 1.5 K. Note that the peak indexed as (110) in Figure 3 corresponds to the (010) peak in the smaller unit cell of $YCa_3(MnO)_3(BO_3)_4$, for which Li and Greaves observed a significant increase in intensity below 7.5 K. Given that this peak is extremely weak in the vanadium compound, any similar increase due to magnetic order would be even more evident. We therefore find no evidence for long-range magnetic order in $YCa_3(VO)_3(BO_3)_4$.

Figure 4 shows the temperature dependence of magnetic susceptibility $\chi(T)$ collected in a field of 1 T under zero-field-cooled conditions. Apart from the kink and slight decrease at $T \approx$ 178 K, related to the onset of AFM order in the V_2O_3 impurity phase, no distinct anomalies were observed. Note that the V_2O_3 magnetic transition normally (in bulk) occurs at 150 K; the observed shift of the Néel temperature in this case is probably caused by slight doping or nonstoichiometry.[22] Above this anomaly, $\chi(T)$ follows a Curie−Weiss (CW) law, $\chi(T) = \mu_{eff}^2/8(T - \Theta)$, where μ_{eff} is an effective magnetic moment, and Θ is the Curie−Weiss characteristic temperature. A least-squares fit yields μ_{eff} = 2.88 μ_B/V and Θ = −453 K. The measured effective moment is in excellent agreement with the predicted value 2.83 μ_B for S = 1, as expected for V^{3+}. The large and negative Θ suggests the presence of strong AFM exchange between vanadium ions (Θ being proportional to the average magnetic exchange parameter J) above 180 K. Below the AFM transition of the V_2O_3 impurity phase, $\chi(T)$ does not follow the CW law. As shown in Figure 4, below ∼100 K, an increase in susceptibility compared to the high-temperature CW fit takes place, signaling the appearance of a FM magnetic exchange component in the system.

Analyzing the field dependencies of magnetization $M(B)$ (inset of Figure 4a) confirmed the absence of long-range

dx.doi.org/10.1021/cm1034003 |Chem. Mater. 2011, 23, 1315–1322

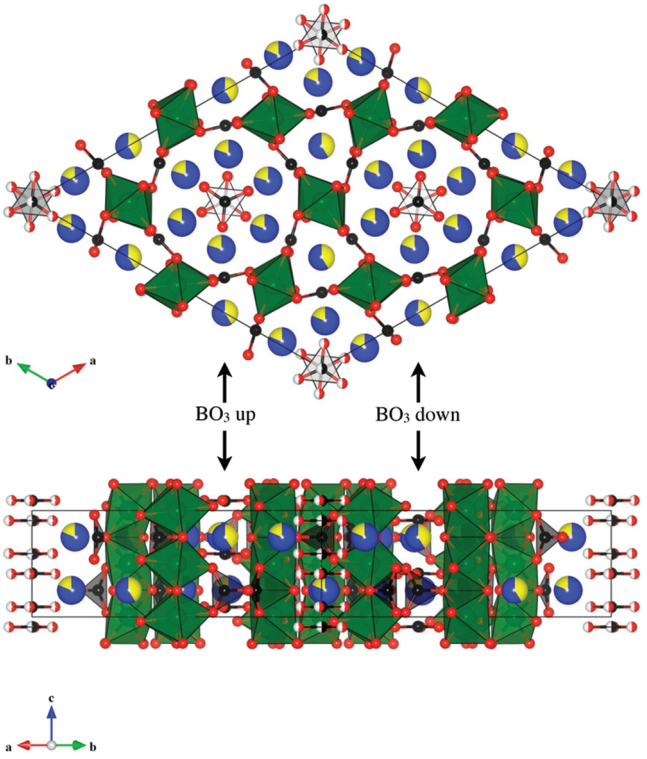

Figure 2. (Color online). Structure of $YCa_3(VO)_3(BO_3)_4$ at 150 K, refined simultaneously against single-crystal neutron Laue and X-ray diffraction data. Yttrium atoms are yellow; calcium atoms are blue; vanadium atoms and VO_6 octahedra are green; boron atoms and BO_3 triangles are black; and oxygen atoms are red. Fractional occupancies are indicated by segmented spheres (white represents vacancies). Arrows indicate columns of isolated BO_3 triangles that are all above or below the kagomé plane; remaining columns of BO_3 triangles are disordered over these two possibilities.

magnetic order above 3 K. At 3, 6, and 10 K, a slight curvature appears, probably related to Brillouin-like saturation of spins at higher magnetic fields, whereas at 20 K, $M \sim B$ linear behavior is recovered. If $YCa_3(VO)_3(BO_3)_4$ is a noninteracting spin system, then its $M(B)$ dependence should be described by the Brillouin function for ideal paramagnets[24]

$$M_{IP}(B) = g\mu_B S((2S+1)/(2S)\cot((2S+1)/(2S))\text{-}1 /(2S)\cot((1\ /\ 2S)x)\ldots \quad (1)$$

where $x = g\mu_B S/k_B T$, g is the electronic g-factor, S is the spin momentum, and k_B is the Boltzmann constant. According to this equation, all the V magnetic moments should be almost saturated at 3 K and magnetic field of 9 T [$M_{IP}(T = 3K, B = 9T) = 1.96\ \mu_B$/V]. Strongly reduced values of M, i.e., $M(3K, 9T) = 0.2\ \mu_B$/V, indicate the presence of strong AFM coupling. Applying the Brillouin function for interacting spins (eq 1, but with $x = g\mu_B S/(k_B T - \Theta_{eff})$, where Θ_{eff} is an effective Curie−Weiss temperature of the spin system), one can reproduce the latter result with an effective Curie−Weiss temperature of $\Theta_{eff}(3K, 9T) = -75$ K, about 1 order of magnitude lower than its high-temperature value of $\Theta = -453$ K (derived from the Curie−Weiss fit). Such a drastic change should be related to the emergence of an additional ferromagnetic contribution to the magnetic coupling at low temperatures. We were not able to fit

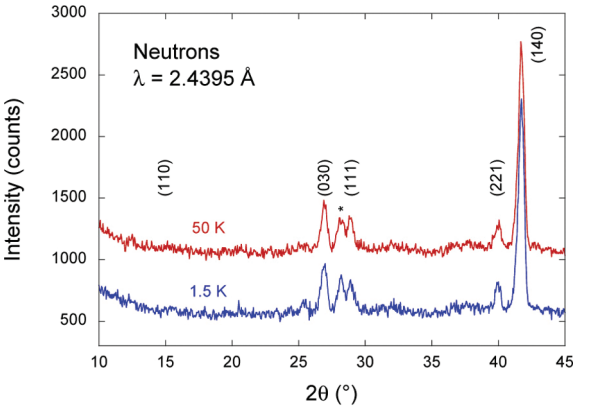

Figure 3. (Color online): Low-angle region of neutron powder diffraction patterns of $YCa_3(VO)_3(^{11}BO_3)_4$ at 50 K (red) and 1.5 K (blue), collected on the Echidna powder diffractometer at the OPAL research reactor, ANSTO. No additional intensity due to magnetic ordering of V^{3+} ions is observed. The peak marked (∗) is the magnetic (010) peak of the V_2O_3 impurity phase.

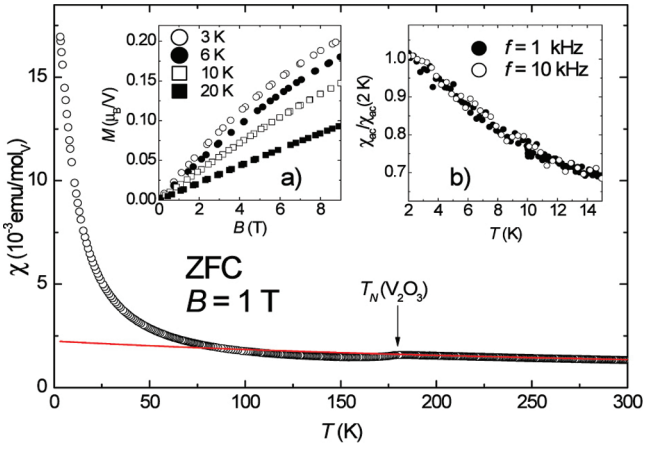

Figure 4. Magnetic susceptibility of $YCa_3(VO)_3(BO_3)_4$. The arrow indicates the Néel temperature of the V_2O_3 impurity. The solid line is the Curie−Weiss fit (for details see the text). The inset in panle (a) shows the field dependence of magnetization $M(B)$ collected at 3, 6, 10, and 20 K, and the inset in panel (b) shows the temperature dependence of the ac susceptibility χ_{ac}.

the $M(B)$ dependence using a Brillouin function for the entire range of B, possibly due to the presence of strong spin frustration. We do not observe any sign of a hysteresis loop opening up.

We also performed low-temperature (down to 2 K) ac susceptibility measurements at 1 and 10 kHz frequencies of the ac magnetic field with an amplitude of 2 Oe. As shown in the inset of panel (b) of Figure 4, there is no sign of a peak or of any frequency dependence of the modulus of the ac susceptibility, $\chi_{ac} = [(\chi')^2 + (\chi'')^2]^{1/2}$, where χ' and χ'' stand for the real and imaginary components of the susceptibility, respectively. The lack of a clear maximum in χ_{ac} is consistent with the results of the NPD experiment described above, with both supporting a complete lack of long-range-ordered magnetism above 1.5 K.

The results of the heat-capacity measurement for $YCa_3(VO)_3(BO_3)_4$ are shown in Figure 5 as a temperature dependence of the ratio C_p/T. The main features of this plot are a distinct

dx.doi.org/10.1021/cm1034003 |Chem. Mater. 2011, 23, 1315–1322

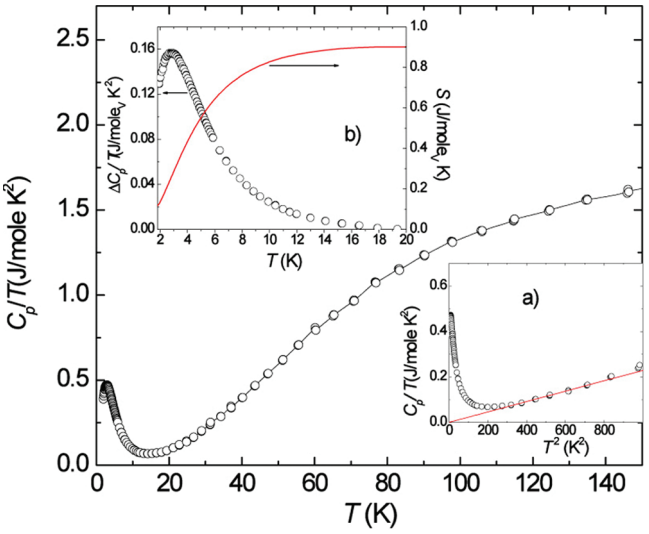

Figure 5. Heat capacity data for $YCa_3(VO)_3(BO_3)_4$ presented as a temperature dependence of the C_p/T ratio. The solid line is a guide for the eye. The inset in panel (a) shows the fit to eq 1, and the inset in panel (b) shows the magnetic contribution to the specific heat and temperature dependence of the magnetic entropy S (for details see text).

maximum at 2.8 K and a further increase due to the lattice degrees of freedom. As shown from the inset in panel (a) of Figure 5, between about 20 and 30 K, the experimental specific heat data can be described by the simple formula

$$\frac{C_p}{T}(T) = \frac{12}{5}\pi^5 \frac{rR}{\Theta_D{}^3}T^2 \qquad (2)$$

where R is the gas constant, r is the number of atoms per formula unit (in this case $r = 26$), and Θ_D is the Debye temperature in the low-temperature limit.[23,24] We do not take any electronic term into account, on the assumption that in the whole temperature range the material is insulating (as it is at room temperature). The derived Debye characteristic temperature from the fit shown in Figure 5(a) is $\Theta_D = 605$ K, which is a reasonable result keeping in mind the large number of light elements such as O and B in the unit cell. Treating the latter result as a lattice contribution to the specific heat in the low-temperature limit, it is possible to estimate the magnetic fraction, $\Delta C_p/T$, as a result of the lattice term extraction from the experimental data below 20 K, which is shown in the inset of panel (b) of Figure 5. One can see that the overall shape of $\Delta C_p/T(T)$ does not resemble lambda-like anomalies typical of first- and second-order phase transitions: the maximum is not sharp, but broad and extended up to 20 K. Magnetic entropy, given by $S(T) = \int_0^T (\Delta C_p/T)dT$ and shown in panel (b) of Figure 5, at 20 K reaches a value of only 0.9 J/mol$_V$ K (assuming $S(0\ \mathrm{K}) = 0$). It is worth noting that the formation of this maximum coincides with the emergence of curvature in the magnetization $M(B)$ dependence.

DISCUSSION

In $YCa_3(MnO)_3(BO_3)_4$ (for which $\Theta = 27.2$ K)[7] and gaudefroyite $Ca_4(MnO)_3(BO_3)_3CO_3$ (for which $\Theta = 45$ K),[8] the positive Θ points to strong FM coupling between transition metal ions within a chain. In contrast, the Curie−Weiss temperature for $YCa_3(VO)_3(BO_3)_4$ is one order of magnitude larger and is negative ($\Theta = -453$ K). The difference and the rapid increase of $\chi(T)$ below 150 K may be explained by two possible scenarios. In the first scenario, using an analogy to $YCa_3(MnO)_3(BO_3)_4$ and $Ca_4(MnO)_3(BO_3)_3CO_3$, the negative Θ is explained by strong AFM interactions within the kagomé plane. The observation that FM coupling arises on subsequent cooling would then be explained by interactions along the chains. However, this scenario seems unlikely when one compares the most probable superexchange paths in the kagomé planes (V−O−O−V) to those in the chains (V−O−V). It is obvious that the shorter path should be preferred, and exchange associated with it should therefore dominate at high temperatures. This leads to the second, more plausible scenario in which the dominant AFM coupling occurs *via* the chains of edge-sharing octahedra (explaining the negative and large Θ), while in the kagomé plane, FM exchange arises at low temperatures (causing the deviation from the CW law and all the features seen in the low-temperature magnetization data). This scenario is consistent with Goodenough−Kanamori rules for transition metals connected at 90° to bridging oxygen ions (via e_g orbitals). Though this interaction is expected to be quite weak for the d^2-d^2 case because of the empty e_g orbital, direct V−V overlap (via t_{2g} orbitals) must be the strongest contribution to AFM exchange along the chains. This is the most important difference between $YCa_3(VO)_3(BO_3)_4$ and its manganese analogue. Direct overlap of d orbitals is enhanced in the V compound by the absence of filled e_g orbitals, which point toward surrounding anions and allow the separation between cations to be minimized.[25] The FM contribution then appears to be associated with in-plane coupling, in contrast with the usual expectations for the kagomé plane. Such a coexistence of in-chain AFM and in-plane FM interactions has been reported for the V^{3+} kagomé compound $NaV_3(SO_4)_2(OH)_6$.[6] Unfortunately, the presence of the V_2O_3 impurity phase does not permit us to test this interplay of FM and AFM interactions with more sophisticated models (based on the Heisenberg Hamiltonian).

An extended bulb-like anomaly of C_p/T at ~2.8 K cannot be attributed to any first- or second-order magnetic phase transitions. This is in agreement with the NPD experiment, which did not find evidence for any magnetically ordered ground state. The strongly reduced value of the entropy associated with this peak—only 10% of $R\ln 3$ predicted for an $S = 1$ system undergoing a long-range magnetic phase transition—may be associated with some kind of short-range magnetically ordered state, which was not detected in dc (down to 3 K) or ac (down to 2 K) susceptibility measurements. One can rule out the presence of spin-glass freezing because in a spin-glass transition, a maximum in $\Delta C_p/T$ should occur above the freezing temperature T_f[26] and should be apparent as a maximum in the ac susceptibility temperature dependence. Because we do not observe frequency-dependent χ_{ac}, a superparamagnetic effect may also be excluded.

Classic magnetically frustrated systems, notably the magnetic pyrochlores which are 3-D realizations of the kagomé lattice, lead to a variety of exotic ground states such as spin-ice ($Ho_2Ti_2O_7$)[27] or spin-liquid ($Tb_2Ti_2O_7$)[28] phases. After exhaustively eliminating all conventional ground states (including spin glass) above, we propose that topological magnetic frustration, together with competition/coexistence of FM and AFM interactions, lead to an exotic magnetic ground state such as spin ice or spin liquid in $YCa_3(VO)_3(BO_3)_4$. Because Li and Greaves[7,8] observed a complex magnetically ordered state in $YCa_3(MnO)_3(BO_3)_4$ below $T_M = 7.5$ K and spin-glass freezing in $Ca_4(MnO)_3(BO_3)_3CO_3$

below T_f = 10 K, we believe that magnetic frustration in our V-based compound is much stronger. The effects of this frustration are puzzling. Further experiments at lower temperatures and on higher-quality samples will be required to resolve the precise character of the ground state.

Finally, we note that the structural details presented in this work—while unprecedented in their detail and revealing a previously unknown superstructure of gaudefroyite-type—offer no additional clues as to the nature of the magnetic exchange pathways of $YCa_3(VO)_3(BO_3)_4$. Each VO_6 octahedron contains two V−O bonds, *trans* to one another, from each of three distinct classes: those involving O atoms shared between two V atoms, forming chains along z [O11−13, 1.865(4)−1.877(5) Å]; those involving O atoms shared between two V atoms and a bridging B atom [O14−16, 2.055(4)−2.069(4) Å]; and those involving O atoms bonded to only one V atom and a bridging B atom [O1−3 and O6−8, 1.977(4)−1.988(4) Å]. Although the differences among these three ranges are statistically significant, they are too small to draw any reliable conclusions about magnetic exchange and are adequately explained by the different bonding environments. In any case, no Jahn−Teller distortions are expected for V^{3+} (d^2). V−V distances are extremely regular [all lying in the range 2.8955(13)−2.9000(13) Å] and offer no clue as to the nature of the metal−metal bonding along the chain (z) direction. The V3−V4 distance, in particular, is constrained by symmetry to be equal; therefore, because we see no evidence for further symmetry lowering in the 1.5 K neutron-diffraction powder or single-crystal data, detailed analysis of the 150 and 1.5 K structures will not yield new information about these bonds. The superstructure is driven by ordering of the isolated columns of BO_3^{3-} triangles, which are highly unlikely to have anything to do with the magnetic exchange pathways. Ca/Y antisite disorder was comparable to that observed in the Mn analogue by Li and Greaves,[7] and we agree with these authors that these isolated sites are equally unlikely to play any role in determining the magnetic ground state.

CONCLUSIONS

$YCa_3(VO)_3(BO_3)_4$ has a gaudefroyite-type structure similar to its Mn analogue $YCa_3(MnO)_3(BO_3)_4$. However, compared to all previously reported gauefroyite-type phases, we have identified a supercell ($\mathbf{a}' = 2\mathbf{a} + \mathbf{b}$, $\mathbf{b}' = -\mathbf{a} - 2\mathbf{b}$, $\mathbf{c}' = \mathbf{c}$) driven by the ordering of columns of BO_3^{3-} anions. The identification and refinement of this supercell is a textbook example of the complementarity of single-crystal neutron and X-ray diffraction data, and it seems likely that single-crystal neutron-diffraction data (if available) would reveal the same weak features in other gaudefroyite-type phases.

We have shown, based on dc susceptibility measurements, that the magnetic exchange in $YCa_3(VO)_3(BO_3)_4$ is dominated by AFM correlations along the 1-D chains of edge-shared VO_6 octahedra at high temperatures, with FM interactions (within kagomé plane) appearing at low temperatures (below ∼100 K). Magnetization and heat-capacity data indicate that the coexistence/competition of FM and AFM correlations, together with geometric frustration, results in a highly frustrated magnetic ground state rather than a conventional long-range-ordered or spin-liquid state. This makes $YCa_3(VO)_3(BO_3)_4$ one of the most highly magnetically frustrated experimental realizations of the kagomé lattice and, therefore, deserving of further study.

ASSOCIATED CONTENT

Supporting Information. ycavbo_x.cif: Crystallographic information file containing X-ray data for the simultaneous refinement of $YCa_3(VO)_3(BO_3)_4$ at 150 K against single-crystal neutron Laue and X-ray diffraction data. ycavbo_n.cif: Crystallographic information file containing neutron data for the simultaneous refinement of $YCa_3(VO)_3(BO_3)_4$ at 150 K against single-crystal neutron Laue and X-ray diffraction data. This material is available free of charge via the Internet at http://pubs.acs.org.

AUTHOR INFORMATION

Corresponding Author

*chris.ling@sydney.edu.au.

Present Addresses

[‖]Department of Chemistry, University of Aarhus, DK-8000 Aarhus C, Denmark

[⊥]Bragg Institute, ANSTO, Locked Bag 2001, Kirrawee DC 2232, Australia

ACKNOWLEDGMENT

This work was supported by the Australian Research Council, Discovery Projects (DP0984585). Financial support for travel to I.L.L. was provided by the Access to Major Research Facilities Programme, which is a component of the International Science Linkages Programme established under the Australian Government's innovation statement, Backing Australia's Ability.

REFERENCES

(1) Anderson, P. W. *Mater. Res. Bull.* **1973**, *8* (2), 153–160.
(2) Fazekas, P.; Anderson, P. W. *Philos. Mag.* **1974**, *30* (2), 423–440.
(3) Anderson, P. W. *Science* **1987**, *235* (4793), 1196–1198.
(4) Grohol, D.; Nocera, D. G. *J. Am. Chem. Soc.* **2002**, *124* (11), 2640–2646.
(5) Papoutsakis, D.; Grohol, D.; Nocera, D. G. *J. Am. Chem. Soc.* **2002**, *124* (11), 2647–2656.
(6) Grohol, D.; Papoutsakis, D.; Nocera, D. G. *Angew. Chem., Int. Ed.* **2001**, *40* (8), 1519.
(7) Li, R. K.; Greaves, C. *Phys. Rev. B* **2003**, *68* (17), 172403.
(8) Li, R. K.; Greaves, C. *Phys. Rev. B* **2004**, *70* (13), 132411.
(9) Kanamori, J. *J. Phys. Chem. Solids* **1959**, *10* (2−3), 87–98.
(10) Li, R. K.; Chen, C. T.; Greaves, C. *Phys. Rev. B* **2002**, *66* (5), 052405.
(11) Ling, C. D.; Neumeier, J. J.; Argyriou, D. N. *J. Solid State Chem.* **2001**, *160* (1), 167–173.
(12) McIntyre, G. J.; Lemée-Cailleau, M. H.; Wilkinson, C. *Phys. B* **2006**, *385*−*386*, 1055–1058.
(13) Campbell, J. W. *J. Appl. Crystallogr.* **1995**, *28*, 228–236.
(14) Campbell, J. W.; Hao, Q.; Harding, M. M.; Nguti, N. D.; Wilkinson, C. *J. Appl. Crystallogr.* **1998**, *31*, 496–502.
(15) Wilkinson, C.; Khamis, H. W.; Stansfield, R. F. D.; McIntyre, G. J. *J. Appl. Crystallogr.* **1988**, *21*, 471–478.
(16) Campbell, J. W.; Habash, J.; Helliwell, J. R.; Moffat, K. *Inf. Q. Protein Crystallogr.* **1986**, *18*, 23–31.
(17) Hoffmann, C.; Armbruster, T.; Kunz, M. *Eur. J. Mineral.* **1997**, *9* (1), 7–19.
(18) Yakubovich, O. V.; Simonov, M. A.; Belov, N. V. *Kristallografiya* **1975**, *20* (1), 152–155.
(19) Petricek, V.; Dusek, M.; Palatinus, L. *Jana2006, The Crystallographic Computing System*; Institute of Physics: Praha, Czech Republic, 2006.

(20) Momma, K.; Izumi, F. *J. Appl. Crystallogr.* **2008**, *41* (3), 653–658.
(21) Brese, N. E.; O'Keeffe, M. *Acta Crystallogr., Sect. B: Struct. Sci.* **1991**, *47*, 192–197.
(22) Mcwhan, D. B.; Menth, A.; Remeika, J. P.; Brinkman, W. F.; Rice, T. M. *Phys. Rev. B* **1973**, *7* (5), 1920–1931.
(23) Gopal, E. S. R. *Specific Heats at Low Temperatures*; Plenum: New York, 1996.
(24) Kittel, C. *Introduction to Solid State Physics*, 8 ed.; Wiley: New Caledonia, 2005.
(25) Goodenough, J. B. *Phys. Rev.* **1960**, *117* (6), 1442–1451.
(26) Martin, D. L. *Phys. Rev. B* **1980**, *21* (5), 1902–1905.
(27) Harris, M. J.; Bramwell, S. T.; Holdsworth, P. C. W.; Champion, J. D. M. *Phys. Rev. Lett.* **1998**, *81* (20), 4496–4499.
(28) Gardner, J. S.; Dunsiger, S. R.; Gaulin, B. D.; Gingras, M. J. P.; Greedan, J. E.; Kiefl, R. F.; Lumsden, M. D.; MacFarlane, W. A.; Raju, N. P.; Sonier, J. E.; Swainson, I.; Tun, Z. *Phys. Rev. Lett.* **1999**, *82* (5), 1012–1015.